Enhanced H-mode pedestal and energy confinement by reduction of toroidal field ripple in JT-60U

H. Urano, N. Oyama, K. Kamiya, Y. Koide, H. Takenaga, T. Takizuka, M. Yoshida, Y. Kamada and the JT-60 Team

Japan Atomic Energy Agency, Naka Fusion Institute, Naka, Ibaraki 311-0193 Japan
e-mail contact of main author: urano.hajime@jaea.go.jp

Abstract. In JT-60U, the pedestal pressure and energy confinement of H-mode plasmas were improved by the installation of ferritic steel tiles (FSTs). The profile of toroidal rotation V_T became less counter with FSTs particularly in case where co-NBI was used at a large volume configuration. In this case, the plasma pressure was raised in a whole range of plasma. At the plasma edge, higher pedestal temperature was obtained with the growth of pedestal width. However, the effect of FSTs became less significant at a small volume configuration. As the V_T became less counter at the pedestal, ELM frequency f_{ELM} was reduced and ELM energy loss ΔW_{ELM} was increased at fixed power crossing the separatrix P_{sep}. In addition, the inter-ELM transport loss is reduced and the pedestal pressure p^{ped} is weakly raised. The effect of FSTs appeared clearly at the large volume configuration where p^{ped} is raised even at a given V_T at the pedestal while p^{ped} is not changed by FSTs at the small volume configuration, suggesting that the reduction of the toroidal field (TF) ripple, the magnitude of which can affect the V_T profile, plays a role in increasing of p^{ped}. For increased p^{ped} due to V_T enhanced in co-direction and the reduction of TF ripple, the spatial width of the pedestal ion temperature became wider. The increase of edge pressure gradient was small when the TF ripple was reduced. The energy confinement was improved with enhancing V_T in co-direction, independently of plasma configuration. Besides, the energy confinement is also improved by the reduction of TF ripple at a given V_T at the large volume configuration.

1. Introduction

The edge pedestal structure characterized by the formation of the H-mode edge transport barrier (ETB) is known to determine the boundary condition of the heat transport in the plasma core as well as the characteristics of the edge-localized-modes (ELMs). In the existing ITER design, the toroidal field (TF) ripple δ_r is estimated as ~1%, where δ_r is defined as the difference of the toroidal magnetic field B_T at the maximum and minimum divided by the averaged B_T. It has been seen empirically that the TF ripple induces the toroidal rotation in the direction counter to the plasma current I_p. It is presumed that in the peripheral region an inward electric field is produced by the losses of fast ions due to TF ripple, which drive the toroidal rotation V_T in the ctr-direction [1]. However, the influence of the TF ripple on the H-mode pedestal structure is not known.

In JT-60U, the ferritic steel tiles (FSTs) were installed in the vacuum vessel to reduce the TF ripple with enhancing the V_T in co-direction in 2005 [2]. It was reported in JT-60U that ELMy H-mode plasmas with V_T in co-direction tend to have higher energy confinement than those in ctr-direction [3]. In the present study, comparing between the plasmas with and without FSTs, the effects of the TF ripple on the pedestal and core confinement properties are examined in JT-60U. In addition, conducting the power scans using the perpendicular NBs for the cases in a variety of the toroidal momentum sources, the characteristics of the H-mode pedestal structure depending on the toroidal rotation is also investigated.

2. Plasma performance after the installation of ferritic steel tiles (FSTs)

In this article, two types of plasma configurations with the plasma volume V_p ~ 52 and 75m^3 are employed, which correspond to δ_r ~ 0.4% and 2.0% at the maximum before the installation of FSTs, respectively. At fixed plasma configuration (V_p ~ 75m^3) with and without

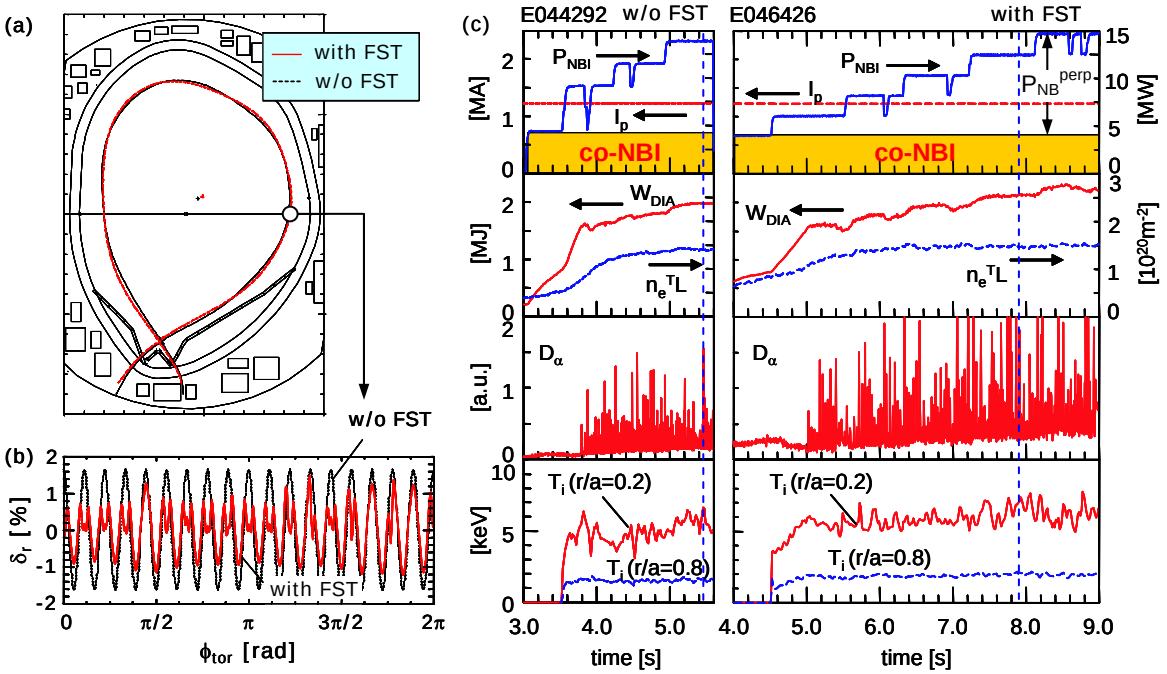

FIG. 1. (a) Plasma boundaries at large V_p configuration ($V_p \sim 75m^3$) with and without FSTs. (b) The amplitude of toroidal field ripple δ_r evaluated at the separatrix on the outer midplane ($B_T = 2.6T$) as a function of toroidal angle ϕ_{tor} with and without FSTs. (c) Temporal evolution of plasma parameters with and without FSTs at the plasma configuration shown in Fig. 1(a) (P_{NBI}: NBI power, W_{DIA}: stored energy measured with a diamagnetic loop, n_e^TL: line-integrated density, D_α: the intensity of D_α emission, T_i: ion temperature measured at r/a=0.2 and 0.8). The toroidal momentum source in co-direction given by the tangential NBs is also indicated as the shadow box. The vertical broken lines are the time slices at which the plasma absorbed power P_{abs} becomes the same at 8.2-8.4 MW for the cases with and without FSTs.

FSTs (see Fig. 1(a)), it is seen that the amplitude of TF ripple is reduced from $\delta_r \sim 1.7\%$ to ~ 1% on the average at the separatrix on the outer midplane by FSTs as seen in Fig. 1(b). Since the FSTs are installed asymmetrically along toroidal direction, the amplitude in TF ripple depends on the toroidal angle. It should be noted that the ripple reduction by FSTs becomes the most effective at $B_T < 2T$ where the fast ion losses become almost half. However, even in higher B_T, the FSTs are still effective (see Fig. 1(b)). For instance, the absorbed power P_{abs} is increased by ~10% with fixed NB injection power at $B_T = 3.2T$. Note that the TF ripple at the small V_p configuration for the case without FSTs is already sufficiently small at $\delta_r \sim 0.35\%$ on the average at the separatrix on the outer midplane. In this case, δ_r is reduced to ~ 0.17% by FSTs.

Shown in Fig. 1(c) are the waveforms of the ELMy H-mode discharges performed at $V_p = 75m^3$ with co-toroidal momentum source. The operational conditions were the same between the discharges with and without FSTs [4], which were performed at $I_p = 1.2MA$ and $B_T = 2.6T$. The safety factor at 95% flux surface q_{95} was fixed at ~ 4.1. The elongation is $\kappa \sim 1.4$ and the triangularity is $\delta \sim 0.35$. For the case of the small V_p configuration ($V_p = 52m^3$), the existing engineering constraint of poloidal field coil currents forces $\delta \sim 0.25$. In Fig. 1(c), after the injection of the tangential neutral beam (NB) adopted as the toroidal momentum source in co-direction, the perpendicular NB injection power was varied in steps during a discharge to keep a wide variation in the fast ion loss. Larger type-I ELM spikes appeared accompanied by lower ELM frequency f_{ELM} and larger energy loss released by each ELM burst ΔW_{ELM} after the installation of FSTs. Detailed analysis on ELM activity is described in Sec. 3.

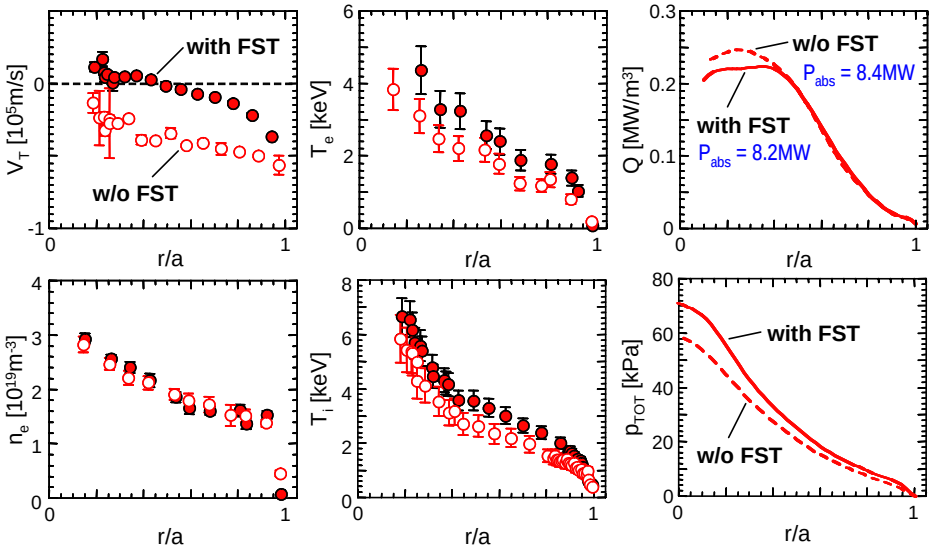

FIG. 2. The profiles of V_T, n_e, T_e, T_i, Q and p_{TOT} for the cases of co-NBI at the large V_p configuration with and without FSTs at P_{abs} = 8.2-8.4MW, where Q denotes the heating power density and p_{TOT} is the total plasma pressure. These profiles correspond to the time slices shown in the broken lines in Fig. 1(c).

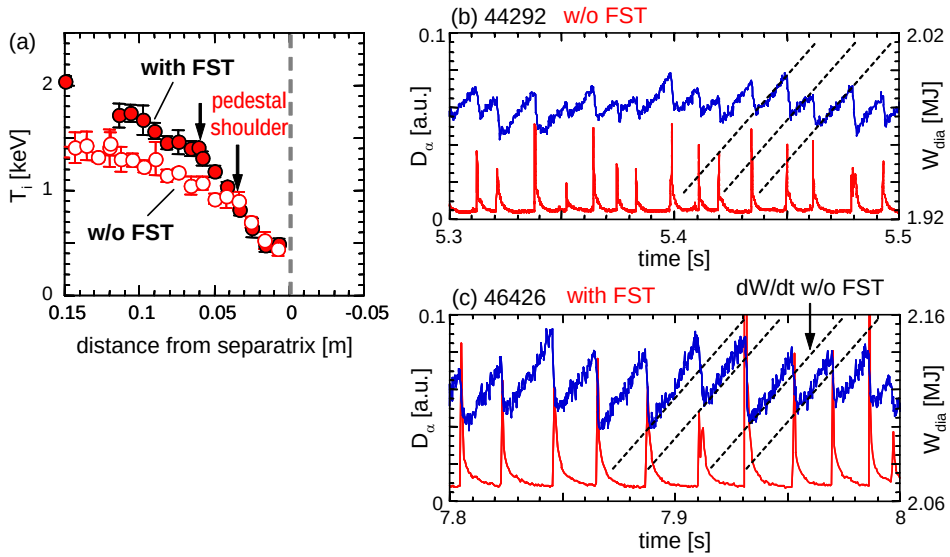

FIG. 3. (a) The T_i profiles in the pedestal region for the cases with and without FSTs, which correspond to the time slices shown in the broken lines in Fig. 1(c). The temporal evolution of D_α emission and W_{dia} for the cases (b) without FSTs and (c) with FSTs. The time derivative of plasma energy dW/dt during the inter-ELM phase for the case without FSTs is shown as broken line.

Radial profiles of the electron density n_e and electron temperature T_e were obtained by Thomson scattering measurement with ruby and YAG laser systems. Ion temperature profile T_i was measured with charge exchange recombination spectroscopy (CXRS) of carbon. The orbit following Monte Carlo (OFMC) code [5] and the tokamak predictive and interpretation code system (TOPICS) [6] were used for the transport analysis of fast ions and thermal plasma.

In Fig. 1(c), time slices at which the values of plasma absorbed power P_{abs} are almost identical at 8.2-8.4MW are shown as broken lines. The NB injection power P_{NBI} is 13.2MW for the case without FSTs, while P_{NBI} is 12.0MW for the case with FSTs. Despite of fixed P_{abs}, the total stored energy W_{DIA} is increased from 1.97MJ without FSTs to 2.18MJ with FSTs.

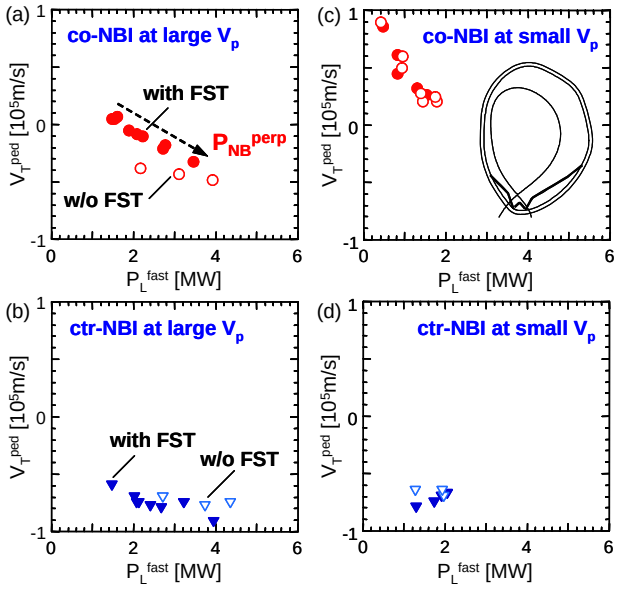

FIG. 4. The relation between the fast ion loss power P_L^{fast} and the toroidal rotation at the pedestal V_T^{ped} for the cases of (a) co- and (b) ctr-NBI at large V_p configuration (V_p ~ 75m^3), (c) co- and (d) ctr-NBI at small V_p configuration (V_p ~ 52m^3). As indicated by broken arrow in Fig. 2(a), P_L^{fast} increases with increasing the perpendicular NBI power P_{NB}^{perp}. The plasma boundary at the small V_p configuration is also shown in Fig. 4(c).

Fig. 2 shows the profiles of V_T, n_e, T_e, T_i, Q and p_{TOT} for the cases with and without FSTs, which correspond to these two time slices shown above. Here, Q and p_{TOT} denote the heating power density and the total plasma pressure, respectively. It is clearly seen that profile of V_T becomes less counter for the case with FSTs at fixed P_{abs}, where the Q profiles are similar with and without FSTs. The n_e profile is not significantly changed while the T_e and T_i are increased in whole range of minor radius, resulting in the increase of plasma pressure.

Fig. 3(a) shows the T_i profiles in the pedestal region for these two time slices. Higher pedestal T_i value is obtained accompanied by wider pedestal width in case with FSTs, while the change in the edge T_i gradient is not clear. Figs. 3(b) and (c) show the ELM activity and its periodic expulsion of plasma energy for the cases without and with FSTs, respectively. By the installation of FSTs, ΔW_{ELM} becomes larger and f_{ELM} decreases. In these figures, f_{ELM} = 70Hz and ΔW_{ELM} = 18kJ at the toroidal rotation velocity at the pedestal V_T^{ped} = -52km/s in case without FSTs while f_{ELM} = 51Hz and ΔW_{ELM} = 34kJ at V_T^{ped} = -21km/s in case with FSTs. In addition, the inter-ELM transport loss is explicitly reduced by FSTs.

With increasing the perpendicular NBI power P_{NB}^{perp}, the fast ion loss power P_L^{fast} is increased. Fig. 4 shows the relation between P_L^{fast} and V_T^{ped} in the power scan using P_{NB}^{perp} for the cases of toroidal momentum source in co- and ctr-direction at the large and small V_p configuration. It is clearly seen particularly in case with co-NBI that V_T^{ped} is directed in counter when the perpendicular NBI power increases the losses of fast ions. It is noted that P_L^{fast} is defined as the sum of the ripple-induced loss, the banana orbit and the charge exchange loss. In case with ctr-NBI, V_T^{ped} is not significantly changed with P_L^{fast}. As is expected, the relation between P_L^{fast} and V_T^{ped} at the small V_p configuration is almost the same for the cases before and after the installation of FSTs. The effect of FSTs on V_T^{ped} is the most remarkable at the large V_p configuration with the toroidal momentum source in co-direction (see Fig. 4(a)). The change in V_T^{ped} in case with ctr-NBI is not as large as that with co-NBI even at the large V_p configuration. It is noted that the shift of V_T^{ped} in counter with the increase of fast ion loss tends to be steeper when V_T^{ped} at the limit of P_L^{fast} = 0 is larger in co-direction. For example, in the small V_p configuration, V_T^{ped} is enhanced in ctr-direction rapidly with increasing P_L^{fast} although the effect of FSTs is negligible. In the H-mode plasmas, a large edge pressure gradient itself is related to the toroidal rotation from the viewpoint of the momentum balance equation [7]. The influences of the ctr-rotation induced by fast ion loss and the viscosity due to large TF ripple without FSTs should be quantitatively evaluated in next step study.

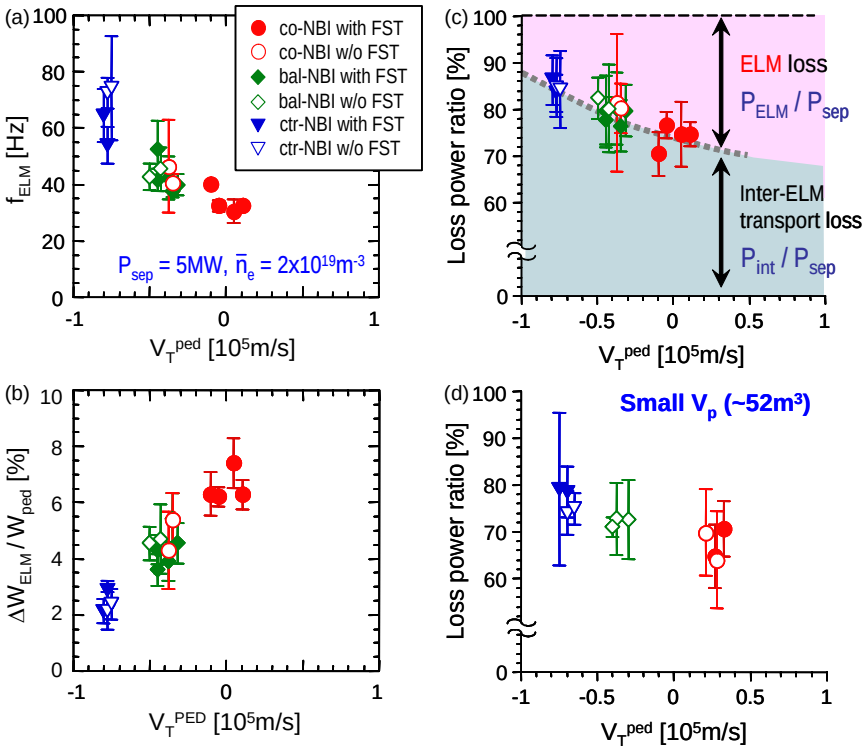

FIG. 5. Dependence of (a) f_{ELM}, (b) $\Delta W_{ELM}/W_{ped}$ on V_T^{ped} in the type-I ELMy H-mode plasmas for the case at the large V_p configuration ($V_p \sim 75m^3$) with fixed power crossing the separatrix P_{sep} (= 5MW) and line-averaged electron density $\bar{n}_e$ (=2x10^{19}m^{-3}), where W_{ped} denotes the pedestal stored energy. The loss power ratio of intra- (P_{ELM}/P_{sep}) and inter-ELM transport (P_{int}/P_{sep}) as a function of V_T^{ped} at (c) the large and (d) small V_p configurations ($V_p \sim 52m^3$), where P_{ELM} denotes the ELM loss power and P_{int} is the inter-ELM loss power.

3. Effects of toroidal field ripple and toroidal rotation on ELMs and pedestal structure

In Sec. 2, it is shown that the pedestal and total energy confinement are improved by the installation of FSTs. However, it is not clear whether this improvement is attributed to the reduction of TF ripple or the shift of toroidal rotation in relatively co-direction by the installation of FSTs. In this section, in order to decouple the effects of the TF ripple and toroidal rotation, the dependence of pedestal parameters on one of these two is examined while keeping the other fixed.

In type-I ELMs, it has been known that f_{ELM} increases in proportion to the power crossing the separatrix P_{sep}. However, power scans using the perpendicular NBs in JT-60U induce the toroidal rotation in ctr-direction as shown in Fig. 4. Therefore, the power dependence of ELM frequency in JT-60U involves in many cases the effect of toroidal rotation. Fig. 5(a) shows f_{ELM} in the type-I ELMy H-mode plasmas as a function of V_T^{ped} at a given P_{sep} (= 5MW) for the case of the large V_p configuration. Despite of fixed P_{sep}, it can be clearly seen that f_{ELM} decreases as the toroidal rotation in co-direction is enhanced, independently of the existence of FSTs. In fact, this relation between f_{ELM} and V_T^{ped} was seen before the installation of FSTs [8]. On the other hand, Fig. 5(b) shows the normalized ELM energy loss $\Delta W_{ELM}/W_{ped}$ as a function of V_T^{ped} for the same dataset shown in Fig. 5(a), where W_{ped} denotes the pedestal stored energy. At a given P_{sep}, $\Delta W_{ELM}/W_{ped}$ clearly increases as the toroidal rotation in co-direction is enhanced. Fig. 5(c) shows the dependence of the loss power ratio of intra- (P_{ELM}/P_{sep}) and inter-ELM transport (P_{int}/P_{sep}) on V_T^{ped}, where P_{ELM} denotes the ELM loss

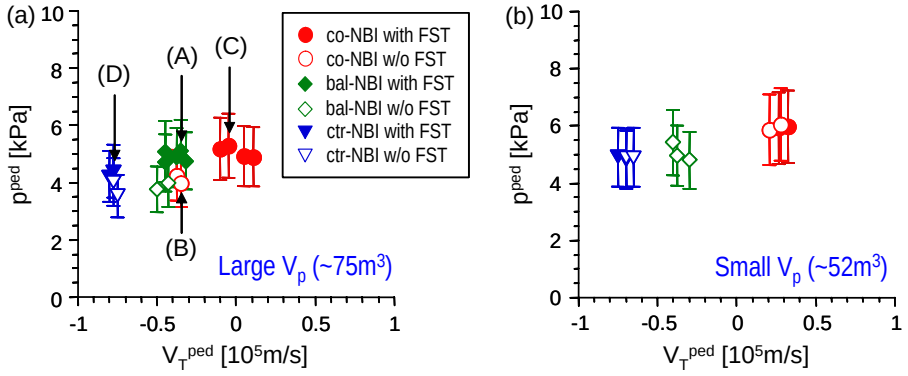

FIG. 6. Dependence of pedestal pressure p^{ped} on V_T^{ped} in the type-I ELMy H-mode plasmas for the cases of (a) the large ($V_p \sim 75m^3$) and (b) small V_p configuration ($V_p \sim 52m^3$) with fixed P_{sep}.

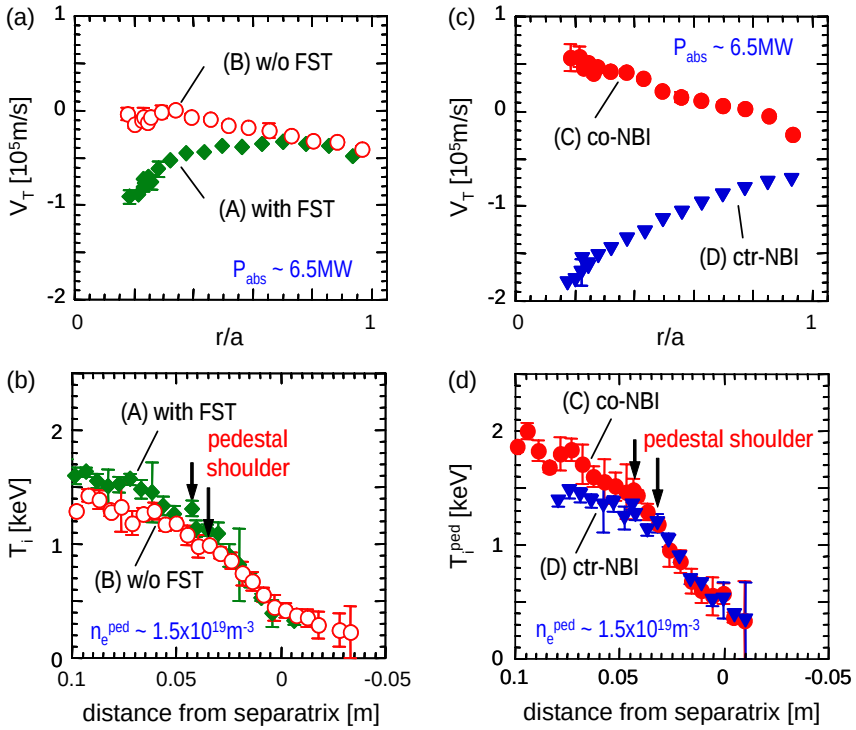

FIG. 7. Profiles of (a) V_T and (b) edge T_i for the cases with and without FSTs at fixed V_T^{ped}. Profiles of (c) V_T and (d) edge T_i for the cases of V_T^{ped} in relatively co- and ctr-direction with FSTs. The cases (A)-(D) correspond to the data indicated in Fig. 6(a).

power defined as $P_{ELM} = f_{ELM} \Delta W_{ELM}$ and P_{int} is the inter-ELM loss power given as $P_{int} = P_{sep} - P_{ELM}$. In this plot, P_{ELM} stays around 15-25% of P_{sep} with the normalized electron-ion collisionality at the pedestal ν* in the range of 0.06-0.14. In JT-60U, the inter-ELM transport is reduced at lower ν* [9]. However, when V_T^{ped} becomes less counter in the narrow range of ν*, the ratio of inter-ELM transport loss power tends to decrease slightly and larger fraction is assigned to the ELM loss power. Besides, the fraction of inter-ELM transport tends to be reduced slightly by the installation of FSTs at a given V_T^{ped} at the large V_p configuration, while the relation between V_T^{ped} and the inter-ELM transport loss power is not explicitly changed by FSTs at the small V_p configuration as shown in Fig. 5(d).

Fig. 6 shows the dependence of pedestal pressure p^{ped} on V_T^{ped} for the cases of the large and small V_p configuration at fixed P_{sep}. It can be seen that p^{ped} increases weakly with the increase of V_T^{ped} in co-direction (see the cases with FSTs in Fig. 6(a)). However, at the large V_p

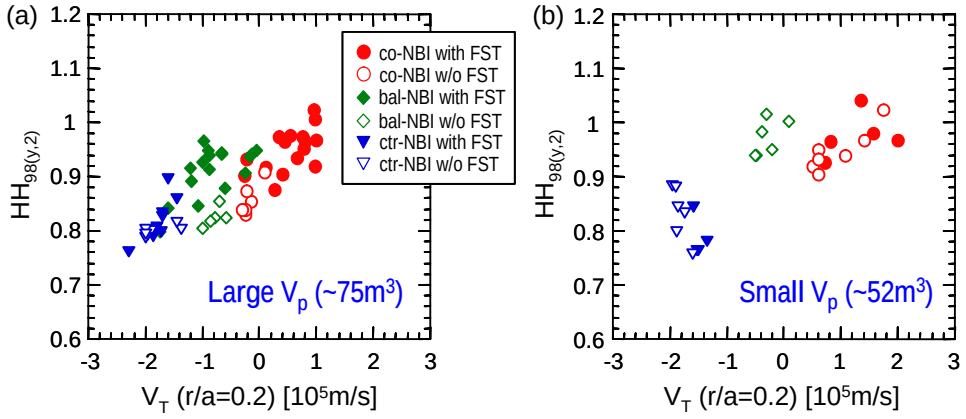

FIG. 8. (a) The HH-factor based on the IPB98(y,2) scaling $HH_{98(y,2)}$ as a function of V_T at r/a=0.2 for the cases of (a) the large V_p configuration and (b) the small V_p configuration.

configuration, p^{ped} is raised by FSTs at a given V_T^{ped}, while the change of p^{ped} by FSTs is not observed at the small V_p configuration. This result suggests that the reduction of TF ripple, the magnitude of which can influence the V_T profile, affects the increase of p^{ped} because the effect of FSTs is less significant at smaller V_p configuration.

It should be then discussed how the pedestal structure is changed by the reduction of TF ripple and by the variation of V_T at the plasma edge. Figs. 7(a) and (b) show the comparison of the profiles of V_T and edge T_i between the plasmas with and without FSTs. As seen in Fig. 7(a), the edge V_T profiles are almost identical. In Fig. 7(b), one can find that the pedestal T_i for the case with FSTs becomes higher with n_e at the pedestal being constant because of the extension of pedestal width and the slight increase of edge T_i gradient. In this case, the energy confinement is also improved by the reduction of TF ripple from $HH_{98(y,2)}$ = 0.85 (without FSTs) to $HH_{98(y,2)}$ = 0.95 (with FSTs), where $HH_{98(y,2)}$ denotes the energy confinement enhancement factor based on the IPB98(y,2) scaling [10]. On the other hand, Figs. 7(c) and (d) show the comparison of the profiles of V_T and edge T_i between the plasmas with V_T^{ped} in relatively co- and ctr-direction with FSTs, i.e. the TF ripple is the same. As seen in Fig. 7(c), the V_T profiles are totally different because the toroidal momentum sources using the tangential NBs head for co- and ctr-direction. In Fig. 7(d), one can find that the pedestal T_i for the case with co-NBI is slightly higher with keeping n_e at the pedestal fixed because the pedestal width becomes wider while the pedestal T_i gradient is not clearly changed by V_T. In this case, $HH_{98(y,2)}$ is raised from 0.80 to 0.98 with enhanced V_T in co-direction.

4. Energy confinement properties

In this section, the effects of the reduced TF ripple and the enhanced toroidal rotation in co-direction on the energy confinement are discussed. Fig. 8(a) shows the dependence of *HH*-factor on V_T at r/a = 0.2 for the case of the large V_p configuration. It is clearly seen that the $HH_{98(y,2)}$ tends to increase with enhancing the core V_T in co-direction. Since the dynamic range of V_T is extended explicitly in co-direction, the effect of toroidal momentum source becomes clearer in case with FSTs. In addition to the influence of V_T, the energy confinement is improved by the reduction of TF ripple at a given V_T, as can be qualitatively expected from the pedestal properties discussed in Sec. 3. For the reference, the dependence of *HH*-factor on V_T at r/a = 0.2 for the case of the small V_p configuration is shown in Fig. 8(b). On the contrary to Fig. 8(a), since the effect of FSTs is small, the relation between the *HH*-factor and the core V_T is not explicitly changed by FSTs as expected.

5. Summary

In this study, comparing between the plasmas before and after the installation of FSTs, the effects of the TF ripple on the pedestal and core confinement properties were examined in JT-60U. In addition, conducting the power scans for a variation of the toroidal momentum sources, the characteristics of the H-mode pedestal structure depending on the toroidal rotation were also investigated.

By the reduction of toroidal field (TF) ripple with FSTs, the profile of toroidal rotation V_T became less counter particularly in case where co-NBI was used at the large V_p configuration. In this case, the plasma pressure was raised in a whole range of plasma. At the plasma edge, higher pedestal temperature was obtained with the growth of pedestal width. However, the effect of FSTs became less significant at the small V_p configuration where the pedestal pressure and the energy confinement were not clearly improved.

As the V_T became less counter at the pedestal, ELM frequency f_{ELM} was reduced and ELM energy loss ΔW_{ELM} was increased at fixed power crossing the separatrix P_{sep}. In addition, the inter-ELM transport loss is reduced and the pedestal pressure p^{ped} is weakly raised. The effect of FSTs appeared clearly at the large V_p configuration where p^{ped} is raised even at a given V_T at the pedestal while p^{ped} is not changed by FSTs at the small V_p configuration, suggesting that the reduction of TF ripple, the magnitude of which can affect the V_T profile, plays a role in increasing of p^{ped}. For increased p^{ped} due to V_T enhanced in co-direction and the reduction of TF ripple, the spatial width of H-mode pedestal became wider. The increase of edge pressure gradient was small when the TF ripple was reduced.

The energy confinement was improved with enhancing V_T in co-direction, independently of plasma configuration. Besides, the energy confinement is also improved by the reduction of TF ripple at a given V_T at the large V_p configuration.

References

[1] KOIDE, Y., et al., in Proc. 14th Int. Conf. Würzburg, 1992, IAEA, Vienna vol. 1 (1993) 777.
[2] SHINOHARA, K., et al., in this conference.
[3] SHIRAI, H., et al., Nucl. Fusion **39** (1999) 1713.
[4] URANO, H., et al., Plasma Phys. Control. Fusion **48** (2006) A193.
[5] TANI, K., et al., J. Phys. Soc. Japan **50** (1981) 1726.
[6] SHIRAI, H., et al., Plasma Phys. Control. Fusion **42** (2000) 1193.
[7] YOSHIDA, M., et al., in this conference.
[8] KAMIYA, K., et al., Plasma Phys. Control. Fusion **48** (2006) A131.
[9] URANO, H., et al., Phys. Rev. Lett. **95** (2005) 035003.
[10] ITER PHYSICS BASIS, Nucl. Fusion **39** (1999) 2175.